Acta Crystallographica Section B
Structural Science
ISSN 0108-7681

Determination of the crystal structure of magnesium perchlorate hydrates by X-ray powder diffraction and the charge-flipping method

Kevin Robertson* and David Bish

Department of Geological Sciences, Indiana University, Bloomington, IN 47405, USA

Correspondence e-mail: kevrober@indiana.edu

Received 26 January 2010
Accepted 4 October 2010

X-ray powder diffraction (XRD) data were used to solve the crystal structures of phases in the magnesium perchlorate hydrate system, $Mg(ClO_4)_2{\cdot}nH_2O$ (n = 4, 2). A heating stage and humidity generator interfaced to an environmental cell enabled *in-situ* XRD analyses of dehydration reactions under controlled temperatures and partial pressures of H_2O (P_{H_2O}). The crystal structures were determined using an *ab initio* charge-flipping method and were refined using fundamental-parameter Rietveld methods. Dehydration of magnesium perchlorate hexahydrate to tetrahydrate (348 K) results in a decrease in symmetry (space group = $C2$), where isolated Mg^{2+} cations are equatorially coordinated by four H_2O molecules with two $[ClO_4]^-$ tetrahedra at the apices. Further dehydration to the dihydrate (423 K) leads to bridging of the isolated packets to form double corner-sharing chains of octahedra and polyhedra (space group = $C2/m$).

1. Introduction

Perchlorate anions were recently identified on the surface of Mars (Hecht *et al.*, 2009) by the microscopy, electrochemistry, and conductivity analyzer (MECA; Kounaves *et al.*, 2010) on the NASA Phoenix lander, which landed in the northern plains of Mars on 25 May 2008. The existence of perchlorate salts in surface deposits on Mars is significant because these hydrates have the potential to be used as indicators of past hydrological cycles (Kounaves *et al.*, 2009). Knowledge of the crystal structures and the effects of temperature and relative humidity (RH) on perchlorate hydrates is required in order to predict phase stabilities and to understand the reactivity of the martian soil in terms of H_2O cycling between the regolith and the atmosphere on Mars.

Perchlorate $[ClO_4]^-$ ions contain chlorine in the VII oxidation state, making them very strong oxidants. Perchlorate salts are highly reactive and are commonly used in pyrotechnics, rocket propellants, flares and fertilizers (Parker, 2009). Chlorine occurs in these salts in tetrahedral coordination with oxygen along with cations such as Na, Mg, Ca, Ni and Zn coordinating with as many as six H_2O molecules. The salts are typically hygroscopic and rapidly deliquesce when exposed to humid conditions, making them very rare on the Earth's surface except in arid regions. Ericksen (1983) reported high concentrations of perchlorate in Chilean nitrate deposits from the Atacama Desert, believed to be of atmospheric origin (Michalski *et al.*, 2004). Perchlorate minerals have also been reported in playa deposits of the southwestern United States (Rao *et al.*, 2007; Kounaves *et al.*, 2009) and most recently in the Antarctic Dry valleys in concentrations up to 1100 μg kg^{-1} (Kounaves *et al.*, 2010).

As described by West (1934), the $Mg(ClO_4)_2{\cdot}6H_2O$ structure is orthorhombic ($Pmn2_1$) and each Mg^{2+} cation is octahedrally coordinated by H_2O molecules. Perchlorate tetrahedra form two rings of three tetrahedra each around the octahedra in the (001) plane (Ghosh *et al.*, 1997). These tetrahedra are presumably hydrogen-bonded to the Mg octahedra, although the H positions have not been determined. Three dehydration products of the hexahydrate phases (H_2O = 4, 2, 0) were reported by Besley & Bottomley (1969) using a vapor pressure equilibrium technique and these were later confirmed by Devlin & Herley (1986) using thermogravimetric analysis (TGA) and XRD. They reported the existence of distinct X-ray diffraction patterns, suggesting the occurrence of structural changes resulting from the evolution of H_2O. However, the crystal structures have not been reported in the literature.

In this paper we describe the solution and refinement of the $Mg(ClO_4)_2{\cdot}nH_2O$ (n = 4, 2) crystal structures from X-ray powder diffraction data using an *ab initio* charge-flipping method and subsequent fundamental-parameter Rietveld refinement.

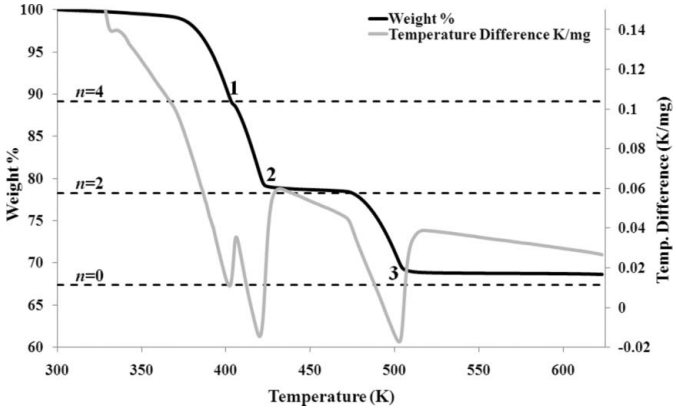

Figure 1
DSC-TGA data for ∼ 20 mg of $Mg(ClO_4)_2{\cdot}6H_2O$ heated from 323 to 573 K at a rate of 2° min^{-1} in a 100% N_2 atmosphere. DSC endotherms (downward inflections in the temperature difference curve) were observed at 403, 423 and 503 K, correlating with the cumulative loss of two, four and six H_2O molecules.

2. Experimental

2.1. Sample preparation

Reagent-grade magnesium perchlorate hexahydrate (99.0%, Alfa Aesar) was ground dry in an agate mortar and pestle and stored in a desiccator prior to analysis.

2.2. Thermogravimetric analysis

Thermal analysis of the Mg perchlorate system was conducted with a simultaneous differential scanning calorimeter-thermogravimetric analyzer (DSC-TGA) from TA instruments (SDT 2960) on ∼ 20 mg of the hexahydrate form to evaluate the dehydration behavior and determine the H_2O content of the subsequent phases. Samples were heated from 298 to 673 K at a rate of 2 K min^{-1} under a 100% N_2 atmosphere (Fig. 1). The hexahydrate phase was also evaluated using a Hiden IGASorp CT TGA instrument, capable of measuring H_2O adsorption and desorption isotherms from ∼ 276 to 598 K at P_{H_2O} values from ∼ 0 to 520 mbar.

2.3. Powder diffraction

Powder samples for XRD measurements were mounted in a cavity specimen mount in an Anton-Paar TTK 450 heating stage on a Bruker D8 Advance diffractometer with Cu $K\alpha$ radiation and a Vantec position-sensitive detector. The heating stage was interfaced with an automated Instruquest VGen RH generator to allow simultaneous control of temperature and P_{H_2O}. *In situ* heating and precise control of P_{H_2O} permitted a systematic study of the dehydration products of the magnesium perchlorate hydrate system. Preliminary heating studies on the diffractometer were performed from 298 to 673 K at a rate of 2 K min^{-1} under a roughing-pump vacuum (∼ 0.15 mbar, equivalent to ∼ 0.01%RH). During heating, a sequence of XRD measurements was made between 21 and 27° 2θ (Fig. 2) to determine the conditions where reactions had gone to completion. Higher-resolution data (10–110° 2θ, 0.0167° steps, 10 s per step) were collected at 348, 423 and 523 K for structure solution of the various hydrate phases.

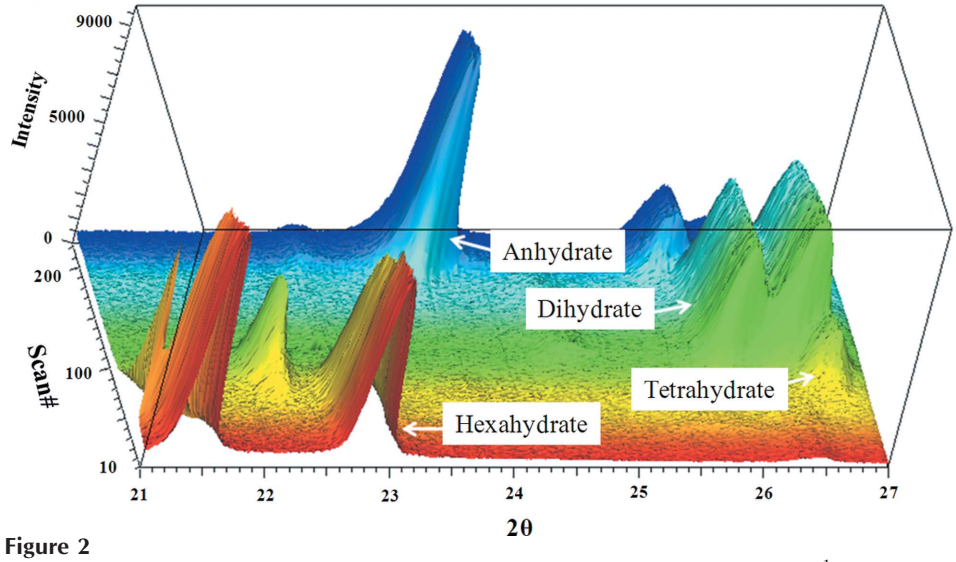

Figure 2
Sequence of XRD measurements between 21 and 27° 2θ. Heating at a rate of 2° min^{-1} at < 1% RH, sequential dehydration was observed, with the anhydrate observed at the highest temperature. The vertical axis represents intensity. The 'time' axis represents temperature from 298 to 498 K in 2° min^{-1} increments.

3. Structure solution and refinement

XRD patterns measured at 348 K for $Mg(ClO_4)_2{\cdot}4H_2O$ and at 423 K for $Mg(ClO_4)_2{\cdot}2H_2O$ (Figs. 3 and 4) were selected for structure determination of the $Mg(ClO_4)_2{\cdot}nH_2O$ (n = 4, 2) system.

3.1. Indexing and Le Bail profile fit

Preliminary indexing of the powder diffraction patterns was performed using the single-value decomposition method (Coelho, 2003) in *TOPAS*4.1 (Coelho, 2007). Sixty-seven peaks for $Mg(ClO_4)_2{\cdot}4H_2O$ were selected below 80° 2θ for initial indexing, yielding the space group *C*2 (No. 5) with a goodness-of-fit of 3.18. A Le Bail profile fit (Le Bail, 2008) in *TOPAS*4.1 was performed to extract diffraction intensities and to refine the unit-cell parameters in the space group *C*2, yielding a = 13.0109 (4), b = 8.0034 (29), c = 5.939 (23) Å, β = 125.274 (14)°, V = 505.008 (3) Å^3, and a final R_{wp} value of 0.084.

Indexing of the data for $Mg(ClO_4)_2{\cdot}2H_2O$ was performed using 58 diffraction peaks below 80° 2θ, yielding the space group *C*2 (No. 5) with a goodness-of-fit of 9.86. Further evaluation of the data supported the space group *C*2/*m* (No. 12). A subsequent Le Bail profile fit using *C*2/*m* yielded a = 14.3819 (4), b = 5.2169 (1), c = 5.4356 (14) Å, β = 108.2011 (14)°, V = 387.427 (18) Å^3, and a final R_{wp} value of 0.051.

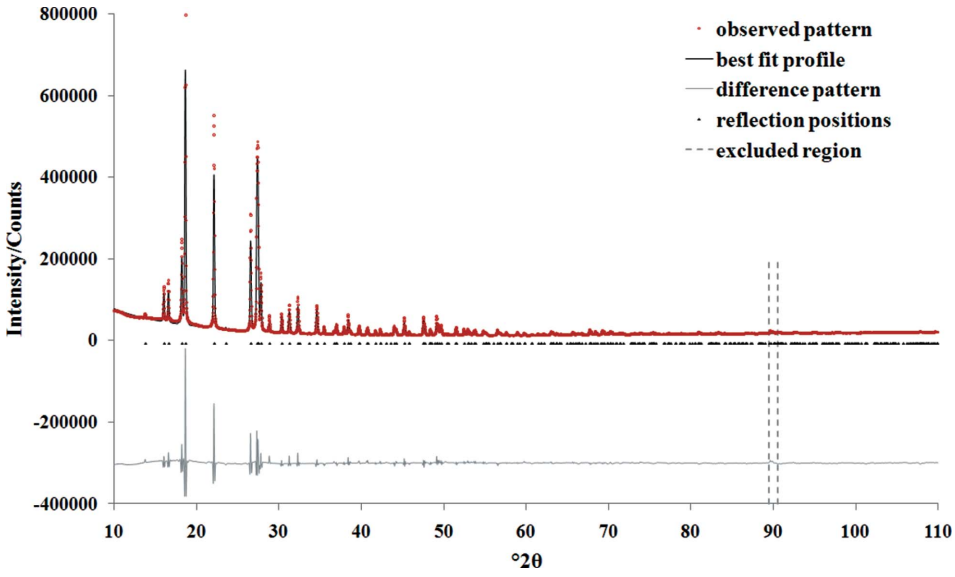

Figure 3
Rietveld refinement results for $Mg(ClO_4)_2{\cdot}4H_2O$ at T = 348 K. Observed profile (red circles), best-fit Rietveld refinement profile (black line), difference pattern (gray line), reflection markers (triangles) and excluded regions (stippled line) are shown. This figure is in color in the electronic version of this paper.

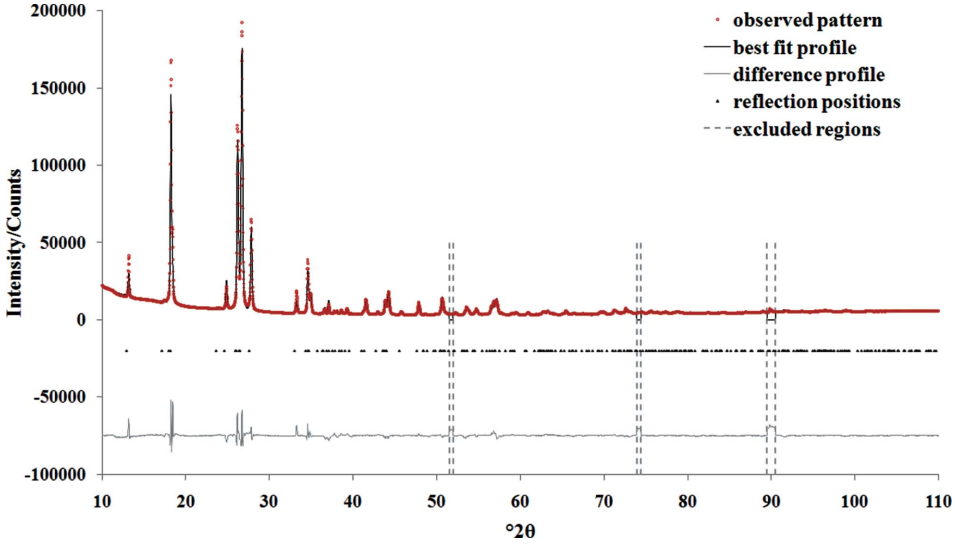

Figure 4
Rietveld refinement results for $Mg(ClO_4)_2{\cdot}2H_2O$ at T = 423 K. Observed profile (red circles), best-fit Rietveld refinement profile (black line), difference pattern (gray line), reflection markers (triangles) and excluded regions (stippled line) are shown. This figure is in color in the electronic version of this paper.

3.2. Charge-flipping structure solution

Crystal-structure solution of the dehydrated phases in this system is difficult using single-crystal techniques owing to the tendency of the material to form an amorphous liquid phase (Devlin & Herley, 1986) before recrystallization. In addition, dehydration of the hexahydrate phase to lower hydrates results in a large volume decrease, producing a mosaic crystal from the original single crystal. Crystal-structure solution using powder XRD data has become a practical alternative to single-crystal methods; however, a solution must deal effectively with the phase problem as well as the degeneracy problem. Charge flipping (Oszlányi & Sütő, 2004, 2005) is a novel technique that uses an iterative method, switching from real to reciprocal space to overcome phase problems. Wu *et al.* (2006) described a Le Bail-like procedure incorporated into the charge-flipping method that solves the degeneracy problem through spherical averaging of overlapping Bragg reflections. This combined charge-flipping algorithm included in *TOPAS*4.1 is described in Coelho (2007) and is often capable of solving complex structures with diffraction data of low resolution.

Charge-flipping parameters and results are presented in Table 1. Reflections where d < 1.0 Å were

Table 1
Charge-flipping parameters and output results.

	$Mg(ClO_4)\cdot 4H_2O$	$Mg(ClO_4)\cdot 2H_2O$
d-spacing limit (Å)	< 1.25	< 1.25
Deleted reflections (#)	16	23
Total reflections (#)	288	247
Weak reflections (#)	210	172
Symmetry restraint	0.9	0.9
Structure factors	82	62
Iterations (#)	351	1630
Time (s)	3	7
R	0.486	0.455

omitted in all analyses. Exclusion of high-angle reflections in lower resolution powder data does not affect the structure output and significantly increases the speed of computation. Amplitudes of the weak reflections were maintained and a $\pi/2$ phase shift was randomly added to 1/3 of the weak reflections for each iteration. The origin of the unit cell was located and the electron densities were shifted to best match the symmetry. The charge-flipping loop was interrupted if the *R* factor did not decrease for 100 consecutive iterations. Once interrupted, a random phase in the range of $(-\pi,\pi)$ was generated to begin a new cycle. A symmetry restraint of 0.9 was applied to the flipped electron density pixels in accordance with the space-group symmetry, allowing 10% variance of atom positions from the symmetry constraint. As described by Coelho (2007), a combination of direct methods (tangent formula) within the iterative process has been shown to aid in structure solution of difficult structures using low-resolution data with weak reflections. Normalized structure factors (E_h) were used for the tangent formula and 50 triplets were set up for each reflection in order to force convergence.

3.3. Fundamental-parameter Rietveld refinement

Structure models for the two and four hydrates determined using the charge-flipping method were refined using a fundamental-parameter Rietveld approach, applying soft bond-distance constraints in *TOPAS-Academic* (Coelho, 2007). Instrumental parameters (*e.g.* goniometer radius, slit sizes *etc.*) were used to calculate the instrumental contribution to peak profiles, and specimen-related crystallite size and strain-broadening information was extracted from the observed profiles. Diffraction patterns had a small contribution from the Ni—Cr plated copper sample mount, resulting in peaks which were excluded from the refinement (Table 2). The background was modeled using a third-order Chebyshev polynomial. Refined parameters included scale factor, unit-cell parameters, specimen displacement, specimen crystallite size and strain, sixth-order spherical harmonics preferred orientation correction, and atomic positions. Atomic positions were refined using soft constraints applied to the Cl—O (1.45 Å) and Mg—O (2.15 Å) distances and angles. Initial refinement of individual isotropic displacement factors (U_{eq}) resulted in values of Mg = 0.01, Cl = 0.019, H_2O oxygen = 0.02 and O = 0.052, and these displacement factors were subsequently fixed to representative values (O = 0.015, Cl = 0.005 and Mg = 0.01) for the final refinements. Site occupancies were fixed to one. The final Rietveld refinement results are presented in Table 2.[1] Difference-Fourier maps were generated after the soft-constraint refinement to locate the H atoms using *TOPAS-Academic* and the resultant positions were fixed in the final Rietveld refinements.

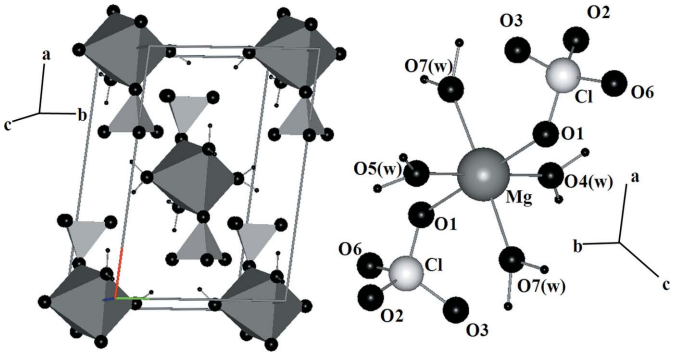

Figure 5
Refined crystal structure of $Mg(ClO_4)_2\cdot 4H_2O$. Mg octahedra are dark grey, ClO_4 tetrahedra are light gray, O atoms are large spheres and H_2O molecules include H atoms (small spheres).

4. Structure description

4.1. Crystal structure of $Mg(ClO_4)_2\cdot 4H_2O$

The refined crystal structure of $Mg(ClO_4)_2\cdot 4H_2O$ is shown in Fig. 5, approximately down the *c* axis. The crystal structure consists of isolated Mg^{2+} ions octahedrally coordinated by $[ClO_4]^-$ anions in the axial positions and H_2O molecules in the equatorial positions. The Mg—O bond lengths of 2.15 (2) Å and Cl—O bond lengths of 1.41 (2) Å are within the ranges expected. The tetrahedral and octahedral bond angles are all within 5% of ideal geometry. The O—H bonds for the H_2O molecules are 1.01 Å with bridging hydrogen bonds (1.84 Å) between the H1 and O6 atoms.

4.2. Crystal structure of $Mg(ClO_4)_2\cdot 2H_2O$

The refined crystal structure of $Mg(ClO_4)_2\cdot 2H_2O$ is shown in Fig. 6 approximately down the *c* axis. Mg^{2+} ions are octahedrally coordinated by two H_2O molecules in axial positions with four $[ClO_4]^-$ anions in bridging equatorial positions. The $[ClO_4]^-$ group shares the 03 and 05 oxygen atoms with adjacent Mg cations, forming double corner-sharing chains parallel to [010], bisecting the *a* and *c* axes. The average Mg—O bond length is 2.123 (4) Å and the average Cl—O bond length is 1.438 (4) Å, with a slightly distorted geometry for both polyhedra. The O—H bond for H_2O is 1.01 Å with long hydrogen bonds (2.68 Å) between the H2 and O4 atoms linking the chains together.

[1] Supplementary data for this paper are available from the IUCr electronic archives (Reference: KD5043). Services for accessing these data are described at the back of the journal.

Table 2
Experimental details.

For all structures: $Z = 2$. Experiments were carried out with Cu $K\alpha$ radiation, $\lambda = 1.54059$ Å using a Bruker diffractometer. H-atom parameters were not refined.

	Profile 1	Profile 2
Crystal data		
Chemical formula	$Cl_2H_8MgO_{12}$	$Cl_2H_4MgO_{10}$
M_r	295.27	255.21
Crystal system, space group	Monoclinic, *C*2	Monoclinic, *C*2/*m*
Temperature (K)	348	423
a, *b*, *c* (Å)	11.4806 (4), 8.0025 (3), 5.9370 (3)	14.3878 (6), 5.2186 (1), 5.4380 (3)
β (°)	112.328 (3)	108.199 (2)
V (Å^3)	504.56 (4)	387.89 (3)
Specimen shape, size (mm)	Flat sheet, 10 × 14	Flat sheet, 10 × 14
Data collection		
Specimen mounting	Ni–Cr plated copper front-loaded sample mount	Ni–Cr plated copper front-loaded sample mount
Data collection method	Reflection	Reflection
Scan method	Step	Step
2θ values (°)	$2\theta_{min} = 10$, $2\theta_{max} = 110$, step size = 0.02	$2\theta_{min} = 10$, $2\theta_{max} = 110$, step size = 0.02
Refinement		
R factors and goodness-of-fit	$R_p = 0.074$, $R_{wp} = 0.104$, $R_{exp} = 0.006$, $R_{Bragg} = 0.058$, $\chi^2 = 226.503$	$R_p = 0.053$, $R_{wp} = 0.078$, $R_{exp} = 0.012$, $R_{Bragg} = 0.036$, $\chi^2 = 38.813$
No. of data points	8383	8383
Excluded regions 2θ (°)	89.5–90.5	89.5–90.5
No. of parameters	52	25
Strain (Lorentzian)	0.0001(1)	0.16 (8)
Crystal size (nm)	>10 000	>10 000

5. Discussion and conclusions

The final refinement results (Figs. 3 and 4) reveal intensity discrepancies associated with the strongest reflections. These discrepancies are likely to be related to the preferred orientation, sample displacement corrections and particle statistics, all of which are related to the *in situ* nature of these measurements. Dehydration of the hexahydrate *in situ* leads to dissolution and re-crystallization, resulting in sample distortion that affects peak positions and likely results in the preferred orientation. Once re-crystallization occurred *in situ*, we had no control over the particle size of the material in the cavity mount, so it is likely not ideal. The final refinements revealed large sample-displacement and spherical harmonic corrections but no significant crystallite-size broadening (Table 2).

Thermogravimetric analyses confirmed three stages of dehydration of the hexahydrate phase, yielding the tetrahydrate, dihydrate and anhydrate phases (Fig. 1). Both TGA and IGAsorp data confirmed that the phase transitions correspond to the evolution of two H_2O molecules each for the tetrahydrate and dihydrate phases. The tetrahydrate phase is the first to form from the hexahydrate, but it is transient and quickly dehydrates to the dihydrate phase. A weight loss of 21.74% in both TGA and IGAsorp data confirms that the dihydrate phase contains two H_2O molecules per formula unit. Devlin & Herley (1986) reported higher temperatures for these phase transitions, but these differences are likely a kinetic effect resulting from more rapid heating rates (10 K min^{-1}) and larger sample sizes used by Devlin and Herley. The transition temperatures and rates of dehydration are also strongly P_{H_2O} dependent, as shown by the IGAsorp data in Fig. 7. The dihydrate phase is stable to $\sim$ 448 K at low RH (<1%) and to $\sim$ 498 K at moderate RH (20%), and above these temperatures it dehydrates almost completely.

The hexahydrate phase resisted dehydration at low temperatures, even under very low P_{H_2O} conditions. The sample was held under vacuum (0.15 mbar) on the XRD stage for 1 week at 273 K with no indication of dehydration until a temperature of at least 323 K was reached. Rehydration experiments at low temperatures (323 K, 0.5% RH) confirmed that the stable phase under these conditions is the hexahydrate phase.

Thermal decomposition of the $Mg(ClO_4)_2{\cdot}nH_2O$ system involves a systematic loss of H_2O molecules, leading to structural rearrangement and a decrease in symmetry. The structure of the hexahydrate phase includes isolated Mg^{2+} cations octahedrally coordinated by H_2O molecules, with hydrogen bonds to isolated $[ClO_4]^-$ tetrahedra that form two-dimensional rings around Mg^{2+}. Heating results in the evolution of two H_2O molecules, causing a reconstructive phase transition as the Mg^{2+} coordination environment is altered. Recoordination of the Mg^{2+} cation and change in symmetry occur as perchlorate anions replace the lost H_2O. The initial removal of two H_2O molecules causes a reduction in symmetry to *C*2, with four H_2O equatorially coordinated to the Mg^{2+}

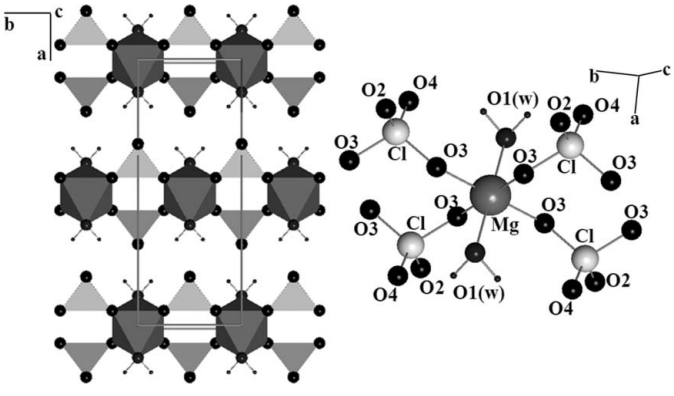

Figure 6
Refined crystal structure of $Mg(ClO_4)_2{\cdot}2H_2O$. Mg octahedra are dark grey, ClO_4 tetrahedra are light gray, O atoms are large spheres and H_2O molecules include H atoms (small spheres).

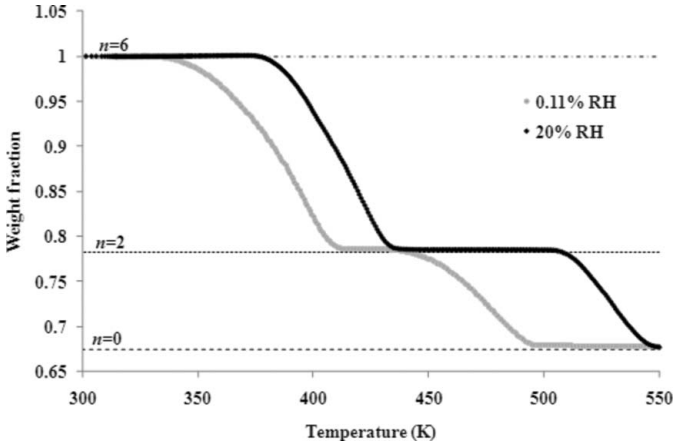

Figure 7
IGAsorp H_2O desorption data for $\sim$ 20 mg of $Mg(ClO_4)_2{\cdot}6H_2O$ heated from 323 to 573 K at a rate of 2° min^{-1} at 0.11% RH (black curve) and 20% RH (gray curve).

cation and two $[ClO_4]^-$ tetrahedra at the apices resulting in isolated packets of polyhedra. Further dehydration to the dihydrate phase leads to bridging of the isolated packets to form chains of octahedra and polyhedra allowing for a mirror plane (space group = $C2/m$). The structure of the anhydrous form has not been solved completely. Based on indexing and charge-flipping structure solution, the structure of the anhydrate appears to have six $[ClO_4]^-$ coordinated to Mg^{2+}, creating an infinite three-dimensional orthorhombic framework. Thus, thermal decomposition involves a transition from isolated polyhedra (n = 6), to isolated clusters (n = 4), to chains (n = 2), and finally to an infinite framework (n = 0) as coordinated H_2O molecules are removed and substituted by perchlorate anions.

Comparison with structurally analogous systems yields similar patterns of decomposition. Sugimoto *et al.* (2007) presented a synchrotron powder diffraction analysis of the dehydration products of bischofite, $MgCl_2{\cdot}6H_2O$. The authors described a similar dehydration process whereby Mg^{2+} ions are initially octahedrally coordinated to H_2O. Dehydration causes removal of H_2O and replacement by Cl in the Mg coordination polyhedron, leading to a transition from isolated octahedra to chains and then to an infinite framework. Another analogous system is the perhennate system $M(ReO_4)_2{\cdot}nH_2O$, where M = Mg, Co, Ni, Cu. Similar to the perchlorates, the ReO_4 ions act as bridging ligands only after H_2O molecules have been removed from the divalent cation coordination sphere. Although the same trends are observed (isolated clusters $\rightarrow$ chains $\rightarrow$ infinite framework), Varfolomeev *et al.* (1994) reported triclinic $P\bar{1}$ symmetry for the $Mg(ReO_4)_2{\cdot}4H_2O$ phase and Butz *et al.* (1998) reported monoclinic $C2/m$ symmetry for $Mg(ReO_4)_2{\cdot}2H_2O$.

The stability of hydrated Mg perchlorate under vacuum is surprising, given its highly reactive nature. Our results thus allow us to predict that under current martian conditions, $Mg(ClO_4)_2{\cdot}6H_2O$ will be the dominant hydrated $Mg(ClO_4)_2$ phase and is unlikely to dehydrate even at the highest surface temperatures on the planet. $Mg(ClO_4)_2{\cdot}6H_2O$ contains 32.6% H_2O, which represents a potential reservoir of H_2O trapped in the regolith that could be cycled into the atmosphere under different obliquity cycles. The distribution and quantity of perchlorate phases on the surface of Mars is still unknown. However, if large playa-type deposits are present, they could represent a significant reservoir of H_2O.

References

Besley, L. M. & Bottomley, G. A. (1969). *J. Chem. Thermodyn.* **1**, 13–19.
Butz, A., Miehe, G., Paulus, H., Strauss, H. & Fuess, H. (1998). *J. Solid State Chem.* **138**, 232–237.
Coelho, A. A. (2003). *J. Appl. Cryst.* **36**, 86–95.
Coelho, A. A. (2007). *TOPAS*, Academic V4.1 Technical reference. http://members.optusnet.com.au/alancoelho.
Devlin, D. J. & Herley, P. J. (1986). *Thermochim. Acta*, **104**, 159–178.
Ericksen, G. E. (1983). *Am. Sci.* **71**, 366–374.
Ghosh, S., Mukherjee, M., Seal, A. & Ray, S. (1997). *Acta Cryst.* B**53**, 639–644.
Hecht, M. H., Kounaves, S. P., Quinn, R. C., West, S. J., Young, S. M. M., Ming, D. W., Catling, D. C., Clark, B. C., Boynton, W. V., Hoffman, J., DeFlores, L. P., Gospodinova, K., Kapit, J. & Smith, P. H. (2009). *Science*, **325**, 64–67.
Kounaves, S. P. *et al.* (2009). *J. Geophys. Res.* **114**, E00A19.
Kounaves, S. P., Stroble, S. T., Anderson, R. M., Moore, Q., Catling, D. C., Douglas, S., McKay, C. P., Ming, D. W., Smith, P. H., Tamppari, L. K. & Zent, A. P. (2010). *Environ. Sci. Technol.* **44**, 2360–2364.
Le Bail, A. (2008). *Powder Diffraction: Theory and Practice*, edited by R. E. Dinnebier & S. J. L. Billinge, pp. 134–165. Cambridge: RSC Publishing.
Michalski, G., Bohlke, J. K. & Thiemens, M. (2004). *Geochim. Cosmochim. Acta*, **68**, 4023–4038.
Oszlányi, G. & Sütő, A. (2004). *Acta Cryst.* A**60**, 134–141.
Oszlányi, G. & Sütő, A. (2005). *Acta Cryst.* A**61**, 147–152.
Parker, D. R. (2009). *Environ. Chem.* **6**, 10–27.
Rao, B., Anderson, T. A., Orris, G. J., Rainwater, K. A., Rajagopalan, S., Sandvig, R. M., Scanlon, B. R., Stonestrom, D. A., Walvoord, M. A. & Jackson, W. A. (2007). *Environ. Sci. Technol.* **41**, 4522–4528.
Sugimoto, K., Dinnebier, R. E. & Hanson, J. C. (2007). *Acta Cryst.* B**63** 235–242.
Varfolomeev, M. B., Zemenkova, A. N., Chrustalev, V. N., Struckov, J. T., Lunk, H. J. & Ziemer, B. (1994). *J. Alloys Compd.* **215**, 339–343.
West, C. D. (1934). *Z. Kristallogr.* **91**, 480–493.
Wu, J., Leinenweber, K., Spence, J. C. H. & O'Keeffe, M. (2006). *Nat. Mater.* **5**, 647–652.